

A Limit-Curve Based Soft Finger god-object Algorithm

Antonio Frisoli [§], Federico Barbagli [†], Emanuele Ruffaldi [§], Kenneth Salisbury [†], Massimo Bergamasco [§]

[†] Stanford University - Robotics Lab
Stanford, CA, U.S.A. - [barbagli,jks]@robotics.stanford.edu

[§] PERCRO - Scuola Superiore S.Anna
Pisa, Italy [a.frisoli,pit,bergamasco]@sssup.it

ABSTRACT

This paper presents a new soft-finger haptic rendering algorithm based on the concept of limit curve which was previously used by the robotic manipulation community to study sliding contacts. The algorithm is more general than the one presented by the same authors in a previous paper since it considers the effects of linear and rotational friction as coupled. However, the solution presented in this paper maintains some of the aspects of simplicity and computational efficiency that characterized the previously proposed solution. To conclude the paper we present a set of simulated interactions between a user and a simple virtual object through a haptic device which allows two point-contact interaction.

CR Categories: I.6.3 [Simulation and modeling]: Applications; I.6.4 [Simulation and modeling]: Model Validation and Analysis;

Keywords: haptic rendering, soft-finger contact, grasping, rotational friction

1 INTRODUCTION AND MOTIVATION

Traditionally, haptic rendering algorithms can be divided into two main categories. Three degrees of freedom algorithms, such as the god-object and the proxy [10, 8] have been extremely popular due to the overwhelming majority of three degrees of freedom devices available on the haptic market and due to their simplicity and computational efficiency. Six degrees of freedom devices [9, 7] simulate a more general type of contact, the one between two generic objects, but tend to be more computationally costly and harder to use given the still limited availability of satisfactory six degrees of freedom haptic devices.

In [3] the authors of this paper proposed a simple extension to the god-object algorithm allowing to simulate a soft-finger contact, i.e. a point-contact with rotational friction constraints. The advantage of this algorithm is that it lets users interact more realistically with a virtual object using two points of contact. In this case, in fact, users are capable of applying form closure to an object, something that they would not be able to do using two point contacts such as the ones simulated by using the god-object and/or proxy algorithms. This extra capability, however, comes at no real additional computational cost, given that collision detection is still point based.

One of the limitations of the algorithm proposed in [3] was to consider the effect of rotational friction and linear friction as two completely uncoupled. This is not the case in reality, as proven for instance by Howe and Cutkosky in [4]. In order to take into account the mutual effect of linear and rotation friction on each other, in this paper we present a soft-finger god-object algorithm based on

the concept of limit curve, which was used in [4] to study robotic sliding manipulation. In the first part of the paper we present the new algorithm and compare it to the simpler one that we presented in the past. In the second part of the paper we present some simulated interactions between two soft fingers and a virtual object obtained using both the above mentioned algorithms. It is important to note that, while in the proposed simulations no additional rotational feedback was physically fed back to the user through the haptic device, the proposed algorithm supports this option.

1.1 Nomenclature

a Radius of the contact area on the fingerpad
 R External radius of the fingerpad undeformed surface
 $p(r)$ Pressure distribution law over the contact area
 P Total normal force applied over the contact area
 M Friction moment induced by normal force P
 q Tangential traction forces over the contact area
 q Tangential traction forces over the contact area
 F_{fr} Global component of tangential traction force due to static/dynamic friction
 M_{fr} Maximum reaction moment due to static/dynamic friction
 F_t Tangential component of force due to static/dynamic friction
 r_m Equivalent friction radius of the tangential friction distribution
 $\mu = \mu_l$ Static and dynamic linear friction coefficient
 μ_r Static and dynamic rotational friction coefficient
 $\Gamma(P)$ Analytical relationship between M and P , approximated to $\mu_r P$

2 TANGENTIAL FORCES AND TORQUES DURING THE CONTROL OF GRIP

During the manipulation of objects our fingertips are generally subjected to tangential torques about the axis normal to the grasp surface in addition to linear forces tangential to the grasp surface. Experimental researches conducted by [5, 6] sensorizing human fingertips during object manipulation have shown as friction tangential forces and torques are linear dependent on the value of the exerted grip force. Our experimental observations [3] confirmed how this relationship could be assumed linear in the range of operating forces during human grip. In particular Johansson et al. [6] reported accurate values of linear and rotational friction coefficients, assuming that the following expressions hold:

$$F_{fr} = \mu_l P \quad (1)$$

$$M_{fr} = \mu_r P \quad (2)$$

More interestingly, from the analysis conducted on different surface materials (rayon, suede, sandpaper), he found that the ratio μ_r/μ_l has a value that is almost independent of the material, as it is reported in table 1. In order to be more general, the relationship between M_{fr} and P can be described also in terms of an analytical function

Surface material	μ_l	μ_r mm	μ_r/μ_l mm
Rayon	0.42 ± 0.07	3.05 ± 0.57	7.39 ± 0.91
Suede	0.61 ± 0.1	3.84 ± 0.74	6.37 ± 0.88
Sandpaper	1.67 ± 0.24	10.11 ± 1.50	6.20 ± 1.54

Table 1: Experimental values of means $\pm SD$ of μ_l , μ_r and their ratio measured at the index fingertip for different materials

Γ according to the model used to describe the elastic properties of the fingerpad, so that expression (2) becomes $M_{fr} = \Gamma(P)$.

This result can be easily explained by analyzing the physics underlying the generation of the friction. In fact the resultant linear and friction forces can be found by integrating the pressure and tangential forces distribution over the fingerpad area during the contact.

Let us assume that the fingerpad is modelled as a sphere, the contact area is assumed to be a circle of radius a , and the pressure distribution is assumed to be axial-symmetric. Under the effect of contact force P , a distribution of pressure $p(r)$ is generated over the contact area, such that:

$$P = \int_0^a p(r) 2\pi r dr \quad (3)$$

Under static conditions, friction forces depend on the friction coefficient μ . In such case p produces on a infinitesimal area dA a tangential traction generating a friction moment M given by:

$$M = \int_0^a \mu_l p(r) 2\pi r^2 dr \quad (4)$$

If we assume that the contact is occurring under limit Hertzian conditions, it can be found that:

$$\frac{\mu_r}{\mu_l} = \frac{M}{\mu_l P} = \frac{3\pi}{16} a(P) \quad (5)$$

Under the hypothesis of uniform distribution of pressure we can find instead:

$$\frac{\mu_r}{\mu_l} = \frac{2}{3} a \quad (6)$$

So the ratio of rotational μ_r to linear friction μ_l is a constant parameter depending on the contact geometry (subject's fingerpad), and can be considered almost independent of the material. Its value is proportional to the radius of the contact area of the fingerpad. A numerical algorithm for the realistic simulation of frictional properties should consider this ratio as a constant independent of the task. So in the remaining analysis, we will adopt the values of linear and rotational friction coefficients derived from table 1.

3 THE EXTENDED SOFT-FINGER GOD-OBJECT ALGORITHM

In the following we will present two algorithms that can be used to simulate the haptic interaction between a set of human fingertips and a virtual object. The first algorithm proposed is simpler to understand and can be easily added on top of pre-existing state of the art haptic rendering algorithms supporting point-contact interaction. The second algorithm is based on more complex mathematical foundations, making it more difficult and harder to implement on top of pre-existing algorithms, but is capable of simulating the interaction between linear and rotational friction effects of the human fingertips in a more realistic way. It is important to note that both algorithms are independent of the type of model chosen to simulate rotational friction between a human fingertip and an object. For a review of possible models see [3].

3.1 The proxy algorithm with uncoupled friction

A 4 DOF god-object can be used to simulate a soft finger contact. Three of such degrees of freedom describe the position that the point of contact would ideally have when touching a virtual object, as for the standard god-object algorithm with linear friction [2]. A fourth variable is added to describe the relative angular motion between the two soft finger avatars and a virtual object. It is important to note that the two parts of the algorithm are disconnected, i.e. they do not influence each other in any way.

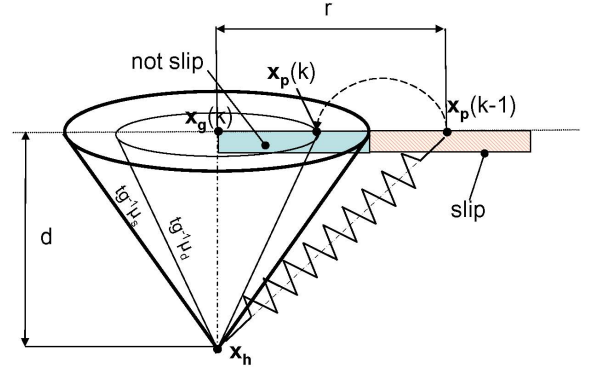


Figure 1: The classical friction cone for simulation of linear friction

When a soft finger avatar comes into contact with a virtual object α_p is set to the current value of the angle describing the rotation of the soft finger avatar α_0 . The position of the haptic interface is described by the position of the HI point \mathbf{x}_h . The following steps are then performed until contact is not broken.

At a generic k -th time sample:

a: Computation of goal position. The new goal position for the god-object is computed as $\mathbf{x}_g = \mathbf{x}_s$, where \mathbf{x}_s is the surface point which minimizes the distance between the HI point \mathbf{x}_h and the contact surface. The new angular position of the users fingers is calculated as $\alpha_g = \alpha_s - \alpha_0$, where α_s is the angular rotation measured by the haptic device.

\mathbf{x}_g and α_g are assumed as the new goal values respectively for \mathbf{x}_p and α .

We assume the following definitions:

$$\begin{cases} r = \|\mathbf{x}_g(k) - \mathbf{x}_p(k-1)\| \\ \rho = |\alpha_g(k) - \alpha_p(k-1)| \\ d = \|\mathbf{x}_g(k) - \mathbf{x}_h\| \end{cases} \quad (7)$$

b: Analysis of the friction condition. In static conditions the new position of the god-object can be expressed as:

$$\begin{cases} \mathbf{x}_p(k) = \mathbf{x}_p(k-1) & \text{if } \frac{|F_t(k)|}{\mu_s |P(k)|} = \frac{r}{\mu_s d} < 1 \\ \alpha_p(k) = \alpha_p(k-1) & \text{if } \frac{|M(k)|}{\Gamma(P(k))} = \frac{k_r \rho}{\Gamma(P(k))} < 1 \end{cases} \quad (8)$$

where $|P| = k_l d$ is the force directed along the contact normal and $\Gamma(P)$ depends on the model chosen for the rotational friction and k_l and k_r are the haptic servo-loop gains, equivalent to a linear and rotational stiffness, used for calculating the elastic penetration force and torque.

If a linear approximation is used for the function $\Gamma(P(k)) = \mu_r P(k)$, then the second condition can be rewritten as:

$$\frac{k_r \rho}{k_l \mu_r d} < 1 \quad (9)$$

Otherwise, conditions of dynamic friction should be applied and the god-object, sliding over the surface, is moved on the boundary of the dynamic friction cone:

$$\begin{cases} \mathbf{x}_p(k) = \mathbf{x}_g(\mathbf{k}) + \mathbf{r}' \\ \alpha_p(k) = \alpha_g(k) + \rho' \end{cases} \quad (10)$$

with

$$\begin{cases} \mathbf{r}' = \frac{\mathbf{x}_p(k-1) - \mathbf{x}_g(k)}{r} \mu_d d(k) \\ \rho' = \frac{\alpha_p(k-1) - \alpha_g(k)}{\rho} \frac{\Gamma(P(k))}{k_r} \end{cases} \quad (11)$$

In case of a linear approximation for the Γ function, the equivalent condition is reduced to:

$$\rho'(k) = \frac{\alpha_p(k-1) - \alpha_g(k)}{\rho} \frac{k_l}{k_r} \mu_r d(k) \quad (12)$$

c: Computation of friction force and torque. A new torque $M(k) = k_r(\alpha_p(k) - \alpha_g(k))$ and a new force $\mathbf{F}(k) = k_l(\mathbf{x}_p(k) - \mathbf{x}_g(k))$ are computed using the new value of α_p and \mathbf{x}_p . Torque $-M(k)\mathbf{v}_n$ and force $-\mathbf{F}(k)$ are applied to the virtual object (where \mathbf{v}_n represents a unit vector with direction along the contact normal). A force $\mathbf{F}(k)$ and a torque $M(k)\mathbf{v}_n$ are also applied to the user (if the device used is capable of actuating such wrench).

d: Computation of the new position of the object. New velocity (\mathbf{v}, ω) and position (\mathbf{x}, θ) is computed for the virtual object. Angle α_c representing how much the object has rotated about axis \mathbf{v}_n is computed as

$$\alpha_c = |\omega \cdot \mathbf{v}_n| \Delta_T \quad (13)$$

where Δ_T is the servo-loop sampling time.

e: Update of god-object position. The current value of α_p and \mathbf{x}_p are corrected to take into account the displacement of the virtual object:

$$\begin{cases} \mathbf{x}_p = \mathbf{x}_p + \mathbf{x}_c \\ \alpha_p = \alpha_p + \alpha_c \end{cases} \quad (14)$$

and then repeat from step a.

4 ANALYSIS OF JOINT APPLICATION OF LINEAR AND ROTATIONAL FRICTION

Considering the effects of linear and rotational friction as completely uncoupled is an approximation of what happens in reality. The limit curve method introduced by [4] is reviewed in this paper to develop an algorithm which takes into account the interplay of these two separate effects.

Refer to Figure 2, where a human fingerpad is represented. When contact with an object arises the distribution of pressure p between fingerpad and object can be assumed to be symmetric. According to the formulation in [4], we will refer to a reference system with origin at the center of symmetry of the pressure distribution p and will consider that the sliding of the fingerpad over the surface can be described as the combination of a translation and rotation

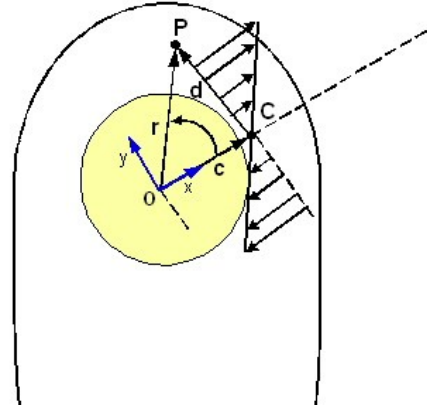


Figure 2: Kinematics of the sliding of the fingerpad over the surface

around the Center of Rotation (COR) C, shown in Figure 2. Another assumption following [4] is that the friction is independent of sliding speed, so that the velocity can be represented aligned along the unit vector:

$$\hat{\mathbf{v}}(x, y) = \frac{[-d_y \ d_x]}{\|\mathbf{d}(x, y)\|} \quad (15)$$

The friction force per unit of surface is so given by the following:

$$\mathbf{q} = \mu_l p \hat{\mathbf{v}}(x, y) dA \quad (16)$$

where we have assumed that $\mu_s = \mu_d = \mu$.

For axisymmetric contacts, if we assume that the x-axis is intersecting the COR, it is possible to express (15) as a function of the distance c of the COR from the origin of coordinates O. For this choice of coordinates, we have also that the resultant force F_x is equal to zero, so that we can limit our computations to M and $F_t = F_y$, where F_t indicates the resultant of the tangential forces. They are given by the following:

$$\begin{cases} F_t = - \int_0^{2\pi} \int_0^R \mu p(r) \frac{(r \cos(\theta) - c)r}{\sqrt{r^2 + c^2 - 2cr \cos(\theta)}} dr d\theta \\ M = - \int_0^{2\pi} \int_0^R \mu p(r) \frac{(r - c \cos(\theta))r^2}{\sqrt{r^2 + c^2 - 2cr \cos(\theta)}} dr d\theta \end{cases} \quad (17)$$

4.1 Computation of the curve limit

Computation of (17) requires a previous knowledge of the pressure distribution on the fingerpad, that is dependent on the mathematical model, adopted for describing the elastic response of the finger. For a given value of applied normal pressure P , a limit curve will describe the analytical relationship between F_t and M .

If we adopt as coordinates a set of dimensionless coordinates F/F_{fr} and M/M_{fr} , only one limit curve can be plotted for each of the mathematical models proposed in [3], as shown in Figure 4, where:

$$\begin{cases} F_{fr} = \mu_l P \\ M_{fr} = \mu_r P \end{cases} \quad (18)$$

When the point $[F_t/F_{fr} \ M/M_{fr}]$ is inside the unitary circle, no sliding can happen between the two bodies. When such condition is not satisfied, both linear and rotational sliding can occur. The maximum friction moment M_{fr} is reached in the condition of purely rotational friction, i.e. a rotation around a fixed point, where the grip is taking place. The maximum linear friction force F_{fr} is reached in the absence of rotational friction, and should satisfy the Coulomb friction law $F_{fr} = \mu_l P$.

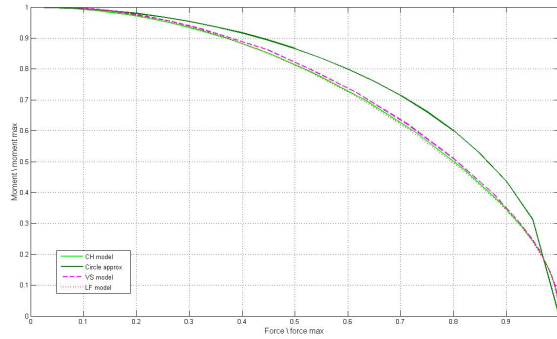


Figure 3: Limit curves associated to different circular pressure distributions. For more details on the pressure distributions see [3].

It can be seen how the models do not present particular differences, and that the limit curve can be approximated by circles with unitary radius in dimensionless coordinates, as shown in Figure 4.

So in the set of coordinates F_t, M , the limit curves can be approximated by a family of ellipses. Figure 4 shows a set of limit curves for different values of the applied normal force P , in the case of Hertzian distribution. The limit curves for $P = \text{const}$ (p -curves) are ellipses with semiaxes given by the maximum friction linear force F_{fr} and momentum M_{fr} according to the applied normal force P .

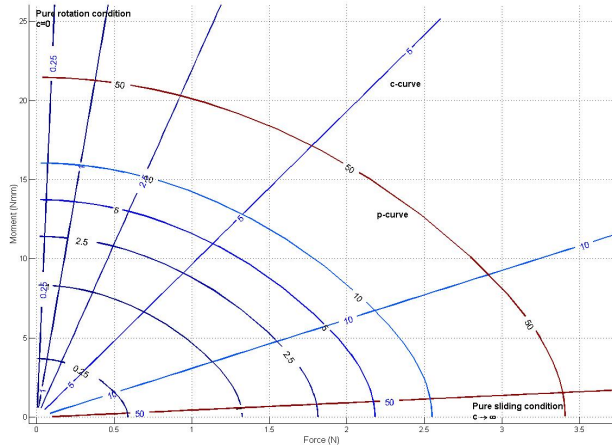


Figure 4: A plot of friction and moment forces for an hertzian distribution

When the gripping force is increased P , the limit curve is shifted toward ellipses with greater semiaxes. For a given gripping force P it is possible to have different sliding motion conditions, described by a different value of c . Also curves with $c = \text{const}$ (c -curves) are displayed in Figure 4. The c -curves are lines departing from the origin that represent friction conditions, where the same sliding movement is taking place between the virtual object and the finger, but with different values of the gripping force P . The two limit conditions are represented by the pure rotation of the object around a fixed point (y coordinate axis corresponding to $c = 0$) and the pure sliding of the object (x coordinate axis corresponding to $c \rightarrow \infty$).

4.2 The extended friction cone

The graphical representation of Figure 4 allows to produce an equivalent interpretation of the friction cone, by extending it to the case of combined rotational and linear friction. The limit condition can be rewritten as:

$$\left(\frac{|F_t(k)|}{\mu|P(k)|}\right)^2 + \left(\frac{|M(k)|}{\Gamma(P(k))}\right)^2 = \left(\frac{r}{\mu d}\right)^2 + \left(\frac{k_r \rho}{\Gamma(P(k))}\right)^2 < 1 \quad (19)$$

Equivalent p -curves and c -curves can be directly traced in the plane $r - \rho$, proving a direct geometric interpretation, useful for the implementation of the algorithm. Condition (19) is simplified when the Γ function is assumed to be $\mu_r P$:

$$\left(\frac{r}{\mu d}\right)^2 + \left(\frac{k_r \rho}{\mu_r k_l d}\right)^2 < 1 \quad (20)$$

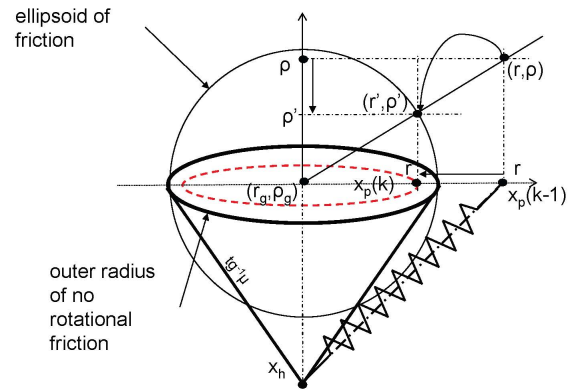


Figure 5: The interpretation of the mixed rotational-linear friction adaptive cone

When condition (20) is not verified, the linear $x_p(k)$ and rotational $\alpha_p(k)$ proxies should be moved on the corresponding p -curve, by computing suitable increments r' and ρ' that satisfy equation (20). The increments r' and ρ' are found as the intersection in the (r, ρ) plane of the c -curve through $[r, \rho]$ with the corresponding p -curve for the level of normal force P , as shown in Figure 5. This shift corresponds to consider that the characteristics of the instantaneous sliding motion are preserved ($c = \text{const}$), but the reaction forces are changed to satisfy the physics of the system.

5 COMBINATION OF LINEAR AND ROTATIONAL FRICTION: THE PROXY ALGORITHM WITH COUPLED FRICTION

Given the elements exposed in section 4, it is now possible to formulate a god-object algorithm that combines linear and rotational friction effects. At a generic k -th time sample, step **b** of previous algorithm is changed to **b'** as follows:

b': Analysis of the friction condition. Compute $\varepsilon = x^2 + y^2$ by:

$$\begin{cases} x = \frac{r}{\mu d} \\ y = \frac{k_r \rho}{\Gamma(P(k))} = \frac{k_r \rho}{\mu_r k_l d} \end{cases} \quad (21)$$

When the god-object is inside the equivalent friction cone, the position of god-object is not changed and so:

$$\begin{cases} \mathbf{x}_p(k) = \mathbf{x}_p(k-1) & \text{if } \varepsilon \leq 1 \\ \alpha_p(k) = \alpha_p(k-1) & \text{if } \varepsilon \leq 1 \end{cases} \quad (22)$$

If $\varepsilon > 1$, the god-object is sliding and the point $[r, \rho]$ is moved to $[r', \rho']$ on the the boundary of the corresponding p -curve, as it is shown in Figure 5. So we have:

$$\begin{cases} \mathbf{x}_p(k) = \mathbf{x}_g(k) + \frac{r'}{r} (\mathbf{x}_p(k-1) - \mathbf{x}_g(k)) \\ \alpha_p(k) = \alpha_g(k) + \frac{\rho'}{\rho} (\alpha_p(k-1) - \alpha_g(k)) \end{cases} \quad (23)$$

6 EXPERIMENTAL VALIDATION AND APPLICATIONS

The algorithm proposed in section 3 has been used in conjunction with a GRAB haptic device [1] allowing two-points interaction with virtual object (see Figure 6). The current design of the device does not allow to recreate contact torques on the users' fingertips. In this scenario the soft-finger algorithm is used solely to compute the effect of the user on the virtual environment. Work is currently being carried out in order to add rotational feedback on the user's fingertips.

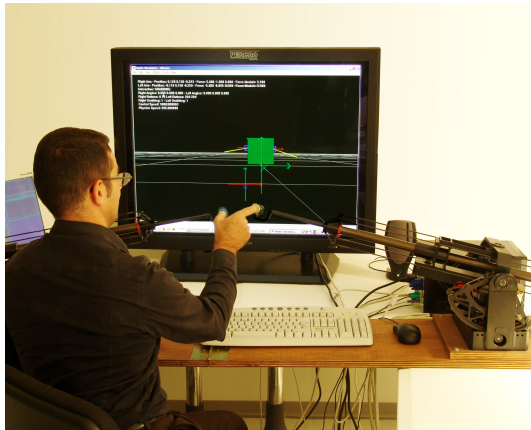


Figure 6: Manipulating virtual objects using two fingers per hand.

The application consisted in the manipulation of a rectangular block, with its center of mass not coincident with the gripping point GP, so that the gravity force exerted a moment with respect to GP. The movements of the block were constrained to the vertical plane, so that only displacements and rotations in this plane were allowed.

The subject was asked to grasp the block on the two opposite planar faces with his two fingers of the same hand, and then to slowly release the pressure between the fingers until the object started sliding. The starting position of the block was horizontal. The subject was instructed to modulate the gripping force in order to achieve a rotation of the object between the fingers, with no or limited sliding. He was allowed to regrip to get out of the sliding state and back into a holding state, when he was not able to achieve a correct rotation of the block.

Different configurations were tested: in particular a class of rayon-suede like materials and sandpaper-like were simulated using the values reported in table 1. Two reference conditions are herewith reported, under the hypothesis of a sandpaper-like material with $\mu_l = 1.67$ and $\mu_r = 10.11$ mm:

Case A: coupled linear and rotational friction;

Case B: uncoupled linear and rotational friction.

Figure 7 represents a typical motion on an object grasped between the fingers, when the grip force is slowly released in condition A. It is easy to see from figures 7 and 8 that there is a translational component of the movement associated to the rotation. Modulating the exerted pressure the subject was able to achieve a smooth rotation of the block with a small amount of translation, as it is visible from the analysis of angle α vs. time, plotted in Figure 8.

The repositioning of the god-object on the p -curves is shown in figure 9. The sliding over the p -curve represents a movement with constant pressure and a reconfiguration of the instantaneous center of rotation. The position of the god-object before repositioning, in dynamic friction conditions, is shown by the diamond black markers: the god-object is then moved on the corresponding p -curve, through the connecting line shown in the same figure. The increase of pressure allows to block the rotation of the object, that is represented by the reaching of the outer p -curve in figure 9, that can provide an adequate value of friction forces to stop the rotation of the object.

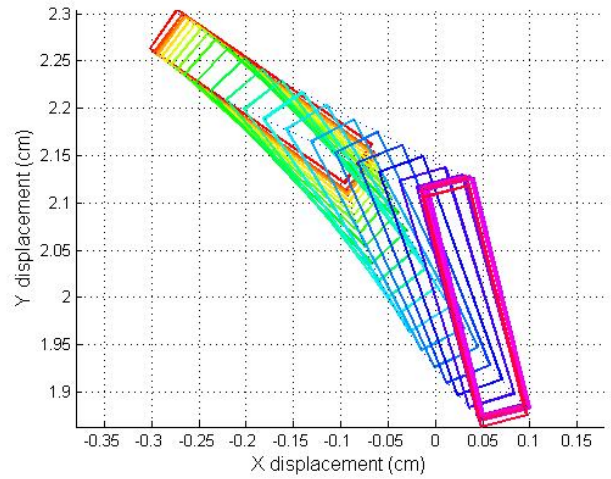


Figure 7: The movement of a rectangle block grasped among two fingers under condition A

In condition B the subject was not able to let the object rotate without sliding between his fingers. From the analysis of Figure 11, it can be seen how the rotation associated to the sliding movement is lower than in condition A and not as much smooth. The resultant motion is shown in Figure 10. The rotation cannot be controlled by the subject, who is holding the object modulating the grip force; at the end the object falls down without changing its initial orientation when the grip force is gradually released by the subject.

These performed tests revealed that using experimental physiological parameters for the friction coefficient, the uncoupled model of friction is unable to simulate a realistic manipulation of objects. The new proposed friction algorithm instead allowed subjects to achieve a good performance in terms of manipulability and control of grip and object orientation.

7 CONCLUSIONS

A god-object based algorithm that models soft finger contact has been proposed based on the limit curve method and an experimental evaluation of the algorithm has been presented. The algorithm can

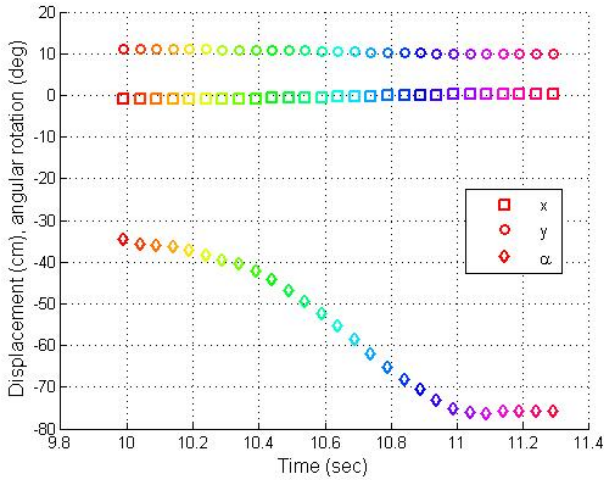


Figure 8: Trajectory vs. time (x and y of CM and rotation α around GP) of the simulated motion under condition A

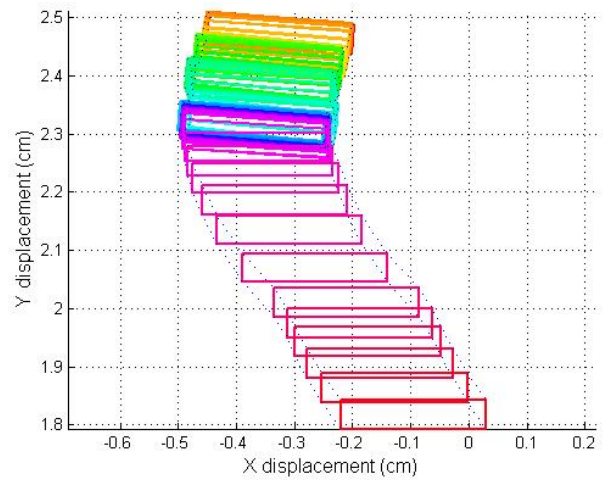


Figure 10: The movement of a rectangle block grasped among two fingers under condition B

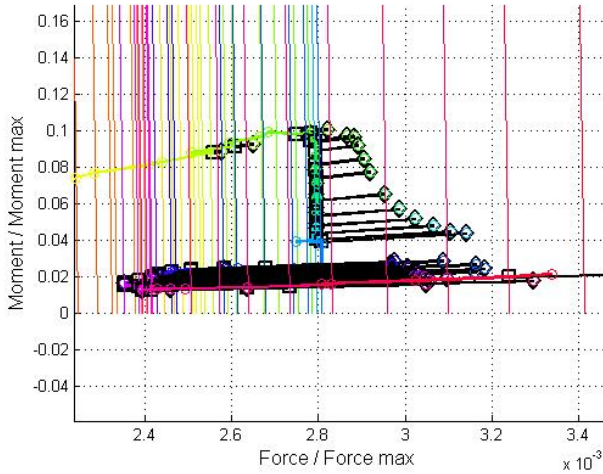


Figure 9: Representation of the repositioning of the god-object in the $[r, \rho]$ plane under condition A

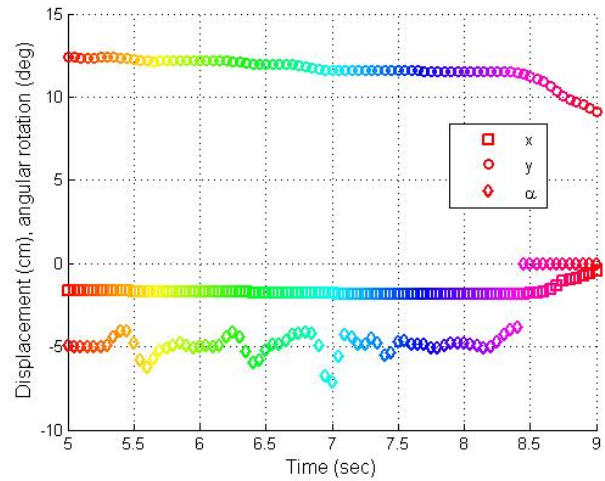


Figure 11: Trajectory vs. time (x and y of CM and rotation α around GP) of the simulated motion under condition B

be easily implemented in real-time and can predict the frictional behavior of a planar object between two soft finger contacts.

8 ACKNOWLEDGMENTS

This work has been possible thanks to the support of the NIH grant LM07295-01 “ Collaborative, Simulation-based, Surgical Training”, Stanford University (Stanford, CA), Scuola Superiore S.Anna (Pisa, Italy).

REFERENCES

[1] Carlo Avizzano, Teresa Gutierrez, Sara Casado, Blaitin Gallagher, Mark Magennis, John Wood, Keith Gladstone, Helen Graupp, Jose A. Munoz, Elena Francisca Cano Arias, and Fiona Slevin. Grab: Computer graphics access for blind people through a haptic and audio virtual environment. In *Proceedings of Eurohaptics 2003*, July 2003.

[2] F. Barbagli, R. DeVengeno, and K. Salisbury. Dual-handed virtual grasping. In *2003 IEEE International Conference on Robotics and Automation, ICRA 2003*, volume 1, pages 1259–1263, Taipei, Taiwan, 2003.

[3] F. Barbagli, A. Frisoli, K. Salisbury, and M. Bergamasco. Simulating human fingers: a soft finger proxy model and algorithm. volume 1, pages 9–17, Chicago, Illinois, March 2004.

[4] R. D. Howe and M. R. Cutkosky. Practical force-motion models for sliding manipulation. *International Journal of Robotic Research*, 15:557–572, 1996.

[5] Johansson R.S. Jenmalm P., Goodwin A.W. Control of grasp stability when humans lift objects with different surface curvatures. *J. Neurophysiol.*, (79):1643–1652, 1998.

[6] H. Kinoshita, L. Backstrom, J. R. Flanagan, and R. S. Johansson. Tangential torque effects on the control of grip forces when holding objects with a precision grip. *J. Neurophysiol.*, (78):1619–1630, 1998.

[7] M. A. Otaduy and M.C. Lin. Sensation preserving simplification for haptic rendering. *ACM Transactions on Graphics*, 22:543–553, 2003.

[8] Diego C. Ruspini, Krasimir Kolarov, and Oussama Khatib. The haptic display of complex graphical environments. *Computer Graphics*,

31(Annual Conference Series):345–352, 1997.

- [9] K. Puterbaugh W. McNeely and J. Troy. Six degree-of-freedom haptic rendering using voxel sampling. In *Proceedings of ACM SIGGRAPH*, page 401408, 1999.
- [10] C. Zilles and J. Salisbury. A constraintbased god-object method for haptic display. In *Proc. IEE/RSJ International Conference on Intelligent Robots and Systems, Human Robot Interaction, and Cooperative Robots*, volume 3, pages 146–151, 1995.